Acta Mech 225, 3103–3113 (2014)
DOI 10.1007/s00707-014-1109-1

Dmitri Kartofelev · Anatoli Stulov

Propagation of deformation waves in wool felt

Received: 12 November 2013 / Revised: 3 February 2014 / Published online: 21 March 2014

Abstract The natural wool felt is becoming increasingly popular and important as a resource material in various applications. In this study, a constitutive equation that describes the deformation wave propagation in the felt material is derived using a hysteretic piano hammer model. A nonlinear partial differential equation with third-order terms that takes into account the elastic and hereditary properties of a microstructured felt is used to study a pulse propagation in the one-dimensional case. The boundary value problem is considered, and the numerical solution describing the strain wave propagation is provided. It is shown that the speed of a deformation wave increases with the growth of its amplitude. Also, the nonlinearity makes the front slope of a pulse steeper, which causes the eventual breaking of a pulse. The solution of the linear problem is analyzed, and the rate of the wave attenuation in the felt material is estimated.

1 Introduction

The felt is likely to be the oldest textile fabric known to man. It is made using wool or other animal fibers by tightly matting them together. Nowadays, wool felt with its unique cellular structure is being used for a wide variety of applications: vibration isolation, sound absorption, noise reduction, filtering, etc. For almost two centuries, the felt has been widely used in the piano manufacturing. For instance, felt pads are used for vibration isolation between vibrating strings and the cast iron frame. Piano dampers are made using wool felt, and of course, the piano hammers are coated with two or several layers of felt.

The first constitutive framework proposed as a mathematical model of the hammer felt was worked out by Ghosh [1], who considered the force–compression characteristic of the felt obeying the power law

$$F = \mathcal{A}u^{\hat{p}}, \quad \mathcal{A} = \text{const}, \tag{1}$$

where F is the acting force, and u is the felt compression. Experimental static testing of different hammers by Hall and Askenfelt [2] demonstrated that for voiced piano hammers, the values of parameter $\hat{p}$ ranging from 2.2 to 3.5 give a good approximation of dependence (1). According to Hertz's law, the force acting on two Hookean bodies gives $\hat{p} = 3/2$. The values of $\hat{p}$ different from $3/2$ indicate the non-Hookean felt properties.

D. Kartofelev (✉) · A. Stulov
Institute of Cybernetics, Tallinn University of Technology, Akadeemia 21, 12618 Tallinn, Estonia
E-mail: dima@cs.ioc.ee
Tel.: +372-55668475
Fax: +372-6204151

A. Stulov
E-mail: stulov@ioc.ee
Tel.: +372-5187079
Fax: +372-6204151

More in-depth information about properties of the hammer felt was presented by Yanagisawa et al. [3] and by Yanagisawa and Nakamura [4,5]. Their dynamic experiments demonstrated very important properties of the felt: The nonlinear force–compression characteristic, strong dependence of the slope of the loading curve on the rate of loading, and the significant influence of hysteresis, i.e., the loading and unloading of the felt, are not alike. The existence of these phenomena requires that the felt is understood as a microstructured material possessing history-dependent properties, or in other words, is a material with memory.

The aim of the current paper was to derive and present a mathematical model that describes the deformation wave propagation in the felt material using the hysteretic piano hammer model. The problem is studied for the one-dimensional case. The presented model takes into account the elastic and hereditary properties of the microstructured wool felt.

2 Compression properties of piano hammer felt

The first dynamical model of the piano hammer felt, which takes into consideration both the hysteresis of the force–compression characteristics and their dependence on the rate of felt loading, was presented in [6]. Following Rabotnov [7], this new nonlinear hysteretic model of the felt was proposed by replacing the parameter $\mathcal{A}$ in expression (1) with a time-dependent operator $F_0[1-\mathcal{R}(t)*]$, where $*$ denotes the convolution operation, and the relaxation function was given by

$$\mathcal{R}(t) = \frac{\gamma}{\tau_0}\,\mathrm{e}^{-t/\tau_0}. \tag{2}$$

Thus, instead of the simple relation (1), the four-parameter hysteretic model of the felt was derived in [6] in the form

$$F(u(t)) = F_0\left[u^{\hat{p}}(t) - \frac{\gamma}{\tau_0}\int_0^t u^{\hat{p}}(\xi)\mathrm{e}^{(\xi-t)/\tau_0}\mathrm{d}\xi\right]. \tag{3}$$

Here, the instantaneous stiffness F_0 and the nonlinearity exponent $\hat{p}$ are the elastic parameters of the material, and hereditary amplitude γ and relaxation time τ_0 are the hereditary parameters. The history of the felt deformation is assumed to start at $t = 0$.

An experimental investigation of the compression characteristics of the piano hammer felt was carried out using a special piano hammer testing device [8,9]. The device was designed for measuring the force and compression histories during a hammer strike against a rigid surface. The aim of these experiments was a verification of the hysteretic model in the form (3), and the determination of the hammer felt parameters.

Figure 1 displays the compression characteristics obtained experimentally. Force–compression curves are presented for three different rates of loading by combining the force and compression histories presented in [9].

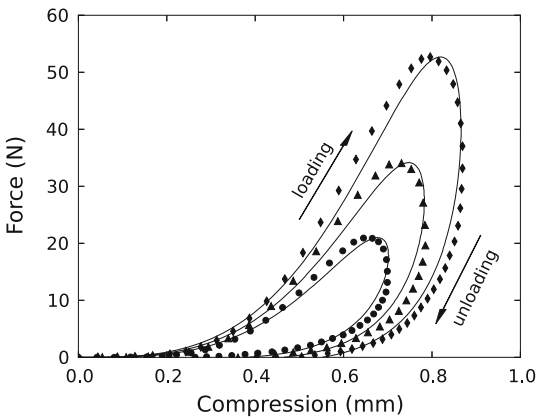

Fig. 1 Comparison of measured data and numerical simulations of force–compression characteristics of the piano hammer. The *arrows* show the directions of the compression and decompression branches. The *symbols* denote measured data for hammer striking velocities: 1.31 m/s (*diamonds*) (contact time $t_c = 1.7$ ms); 1.00 m/s (*triangles*) ($t_c = 2.0$ ms); 0.74 m/s (*bullets*) ($t_c = 2.5$ ms). The *solid lines* are the corresponding curves obtained numerically

The arrows indicate the direction of compression and decompression processes. The solid lines represent the numerical simulation of the experiment, using the four-parameter hysteretic model of the felt in the form (3).

The experimental results presented in Fig. 1 are typical for all measured hammers. A significant influence of hysteresis can be seen clearly in the hammer felt characteristics. The hysteresis leads to the behavior where the loading and unloading of the felt do not follow the same path. This indicates that the energy is dissipating due to viscous damping or frictional losses caused by fiber slippage effects. Moreover, the slope of the force–compression characteristics increases with the growth of the rate of impact, and the contact time is decreased by a stronger strike, exactly like the model of the hysteretic hammer predicts. Thus, we may state that the constitutive four-parameter hysteretic model of the felt describes the dynamic features of piano hammers fairly well and is consistent with the results from experiments presented in [3–5].

The continuous variations in the hammer felt parameters versus key number N were obtained in [9] by numerical simulation of the experimental data for a whole piano hammer set. A best match to the whole set of hammers was approximated using

$$\hat{p} = 3.7 + 0.015\,N, \quad 3.72 \leqslant \hat{p} \leqslant 4.98, \tag{4}$$

$$\gamma = 0.9894 + 0.000088\,N, \quad 0.9895 \leqslant \gamma \leqslant 0.9972, \tag{5}$$

$$\tau_0 = 2.72 - 0.02\,N + 0.00009\,N^2, \quad 1.65 \leqslant \tau_0 \leqslant 2.70, \tag{6}$$

$$F_0 = 15{,}500\,\mathrm{e}^{0.059\,N}, \quad 16{,}440 \leqslant F_0 \leqslant 2{,}787{,}300 \tag{7}$$

for hammer number $1 \leqslant N \leqslant 88$. Here, the unit for relaxation time τ_0 is μs, and the unit for the instantaneous stiffness F_0 is N/mm$^{\hat{p}}$.

The presented regular dependencies of the piano hammer parameters on the key number can be used as a tool for systematical exploration of the process of the hammer–string interaction, or they can be useful for the purpose of improvement of the technological process of the piano hammer manufacturing.

In this study, the aforementioned knowledge regarding the hammer felt compression is used to develop the wool felt model.

3 Wool felt model

In order to analyze the influence of hereditary felt features on the behavior and form of the waves traveling through the felt, the propagation of plane one-dimensional longitudinal wave in an unbounded half-space is considered. The classical equation of motion is in the form

$$\rho \frac{\partial^2 u}{\partial t^2} = \frac{\partial \sigma}{\partial x}, \tag{8}$$

where u is the displacement, σ is the stress, and ρ is the density.

The constitutive equation of microstructured wool felt is derived in a similar manner as the hammer felt model was obtained above. Instead of relation (1), we assume and propose

$$\sigma(\epsilon) = E\epsilon^p(t). \tag{9}$$

Here, $\epsilon = \partial u/\partial x$ is the strain, and E is Young's modulus, and p is the nonlinearity parameter. Because this approach is based on the piano hammer model, we are limited to describe only the compression wave propagation ($\epsilon(x,t) \geqslant 0$).

Following Rabotnov [7] once again, we obtain the constitutive equation of microstructured wool felt by replacing the constant value of Young's modulus E in expression (9) by a time-dependent operator $E_d\,[1 - \mathcal{R}(t)*]$, with the relaxation function in the form (2). This means that for the case of one-dimensional deformation and for any rate of loading, the hysteretic felt material is defined with the aid of the constitutive equation

$$\sigma(\epsilon) = E_d\left[\epsilon^p(t) - \mathcal{R}(t) * \epsilon^p(t)\right], \tag{10}$$

where the constant E_d is the dynamic Young's modulus of the felt. From Eq. (10), it follows that if $t \ll \tau_0$, then we obtain the constitutive equation for the fast felt compression,

$$\sigma(\epsilon) = E_d\epsilon^p(t), \tag{11}$$

and if $t \gg \tau_0$, then we have constitutive equation for the slow compression,

$$\sigma(\epsilon) = E_s \epsilon^p(t). \tag{12}$$

In these two cases, the loading and unloading of the felt occurs in the similar manner. Quantity $E_s = E_d(1-\gamma)$ is the static Young's modulus of the felt material.

Substituting (10) in Eq. (8) and eliminating the integral term lead to the equation in the following form:

$$\rho \frac{\partial^2 u}{\partial t^2} + \rho \tau_0 \frac{\partial^3 u}{\partial t^3} - E_d \left\{ (1-\gamma) \frac{\partial}{\partial x} \left[\left(\frac{\partial u}{\partial x} \right)^p \right] + \tau_0 \frac{\partial^2}{\partial x \partial t} \left[\left(\frac{\partial u}{\partial x} \right)^p \right] \right\} = 0. \tag{13}$$

The analysis of Eq. (13) was reported in [10] where it was shown that the second term of Eq. (13) is significantly smaller compared to the other terms for any reasonable rate of the felt loading (up to 10 m/s). This fact corresponds to the inequality $u \gg \tau_0 |u_t|$, and therefore, the three-parameter model of the felt was derived in [10]. Neglecting the second term of (13), and comparing the new form of Eq. (13) with Eq. (8), one can assume another form of constitutive equation of microstructured wool felt,

$$\sigma(\epsilon) = E_s \left[\epsilon^p + \alpha_0 \frac{\partial(\epsilon^p)}{\partial t} \right], \tag{14}$$

where

$$\alpha_0 = \tau_0/\delta, \quad \delta = 1 - \gamma. \tag{15}$$

Equation (14) is a nonlinear modification of the well-known Kelvin–Voigt model.

Further, this study will consider the equation of motion in its full form (13). The dimensionless form of the equation is obtained by using the nondimensional variables that are introduced by relations

$$u \Rightarrow u/l_0, \quad x \Rightarrow x/l_0, \quad t \Rightarrow t/\alpha_0, \tag{16}$$

where

$$l_0 = c_d \alpha_0 \sqrt{\delta}, \quad c_d = \sqrt{E_d/\rho}, \quad c_s = c_d \sqrt{\delta}. \tag{17}$$

Thus, Eq. (13) in terms of the nondimensional displacement variable $u(x,t)$ takes the following form:

$$\left[(u_x)^p \right]_x - u_{tt} + \left[(u_x)^p \right]_{xt} - \delta u_{ttt} = 0, \tag{18}$$

and for the strain variable $\epsilon(x,t)$

$$(\epsilon^p)_{xx} - \epsilon_{tt} + (\epsilon^p)_{xxt} - \delta \epsilon_{ttt} = 0. \tag{19}$$

Several samples of felt pads made of the same material that is used in piano hammers manufacturing were subjected to the static stress–strain tests. The average value of the static Young's modulus of the pads was estimated to be $E_s = 0.6$ MPa. The average value of the felt density was $\rho = 10^3$ kg/m^3. For realistic results, one should select the values of hereditary parameters γ and τ_0 as follows: $\gamma = 0.99$ and $\tau_0 = 20\,\mu$s. This selection results in the following values of material constants:

$$\delta = 0.01, \quad E_d = 60 \text{ MPa}, \quad c_s = 25 \text{ m/s}, \quad c_d = 250 \text{ m/s}. \tag{20}$$

Using those values of material constants, the space and time scales l_0 and α_0 used in (16) are

$$l_0 = 50 \text{ mm}, \quad \alpha_0 = 2 \text{ ms}. \tag{21}$$

4 Linear case and dispersion relations

Peculiar characteristics of wave propagation in the wool felt are revealed already in the linear case $p = 1$,

$$\epsilon_{xx} - \epsilon_{tt} + \epsilon_{xxt} - \delta\epsilon_{ttt} = 0. \tag{22}$$

The fundamental solution of this equation has the form of traveling waves,

$$\epsilon(x, t) = \hat{\epsilon}\mathrm{e}^{i\kappa x - i\omega t}, \tag{23}$$

where i is the imaginary unit, κ is the wavenumber, ω is the angular frequency, and $\hat{\epsilon}$ is an amplitude. The dispersion law $\Phi(\kappa, \omega) = 0$ of Eq. (22) is defined by the relation

$$i\delta\omega^3 - \omega^2 - i\kappa^2\omega + \kappa^2 = 0. \tag{24}$$

In the case of the boundary value problem, the general solution of Eq. (22) has the following form:

$$\epsilon(x, t) = \frac{1}{2\pi}\int_{-\infty}^{\infty} \Theta(\omega)\mathrm{e}^{i\kappa(\omega)x - i\omega t}\mathrm{d}\omega, \tag{25}$$

where $\Theta(\omega)$ is the Fourier transform of the boundary value of the strain prescribed at $x = 0$,

$$\Theta(\omega) = \int_{-\infty}^{\infty} \epsilon(0, t)\mathrm{e}^{i\omega t}\mathrm{d}t. \tag{26}$$

In case of the initial value problem, the general solution of Eq. (22) has the following form:

$$\epsilon(x, t) = \frac{1}{2\pi}\int_{-\infty}^{\infty} \chi(\kappa)\mathrm{e}^{i\kappa x - i\omega(\kappa)t}\mathrm{d}\kappa, \tag{27}$$

where $\chi(\kappa)$ is the Fourier transform of an initial disturbance of the strain prescribed at $t = 0$,

$$\chi(\kappa) = \int_{-\infty}^{\infty} \epsilon(x, 0)\mathrm{e}^{i\kappa x}\mathrm{d}x. \tag{28}$$

The dependencies $\kappa = \kappa(\omega)$ and $\omega = \omega(\kappa)$ are derived from dispersion relation (24). In general case, κ and ω are complex quantities. In order to provide the dispersion analysis in context with a boundary value problem, we rewrite the wavenumber $\kappa(\omega)$ in the form

$$\kappa(\omega) = k(\omega) + i\lambda(\omega), \tag{29}$$

where $k = \mathrm{Re}(\kappa)$ and $\lambda = \mathrm{Im}(\kappa)$. Using this notation, expression (23) can be rewritten as follows:

$$\epsilon(x, t) = \hat{\epsilon}\mathrm{e}^{i(k+i\lambda)x - i\omega t} = \mathrm{e}^{-\lambda x}\hat{\epsilon}\mathrm{e}^{ikx - i\omega t}. \tag{30}$$

From here, it is clear that for positive values of λ it acts as an exponential decay constant for the spectral components of the wave that is propagating along the positive direction of the space axis. In other words, spectral components decay exponentially as $x, t \to \infty$ for $\lambda(\omega) > 0$. On the other hand, if $\lambda(\omega) < 0$, then the amplitudes of the spectral components grow exponentially as they propagate further along the positive direction of the x-axis. In the latter case, the solution of linear Eq. (22) becomes highly unstable for $t \gg 0$.

5 Dispersion analysis

As discussed above, in order to study the wave propagation along the x-axis, one needs to solve the dispersion relation (24) against wavenumber κ. The solution is in the form

$$\kappa(\omega) = \frac{\omega\sqrt{1 - i\delta\omega}}{\sqrt{1 - i\omega}}. \tag{31}$$

For real values of k and λ, the dispersion relation (24) takes the following form:

$$k^2 + 2ik\lambda - \lambda^2 - ik^2\omega + 2k\lambda\omega + i\lambda^2\omega - \omega^2 + i\delta\omega^3 = 0. \tag{32}$$

In order to study real and imaginary parts separately, the system of equations in the form

$$\begin{cases} k^2 - \lambda^2 + 2k\lambda\omega - \omega^2 = 0 \\ 2k\lambda - \omega(k^2 - \lambda^2) + \delta\omega^3 = 0 \end{cases} \tag{33}$$

is solved and analyzed. Solutions with respect to k and λ are

$$k(\omega) = LM\left(\sqrt{1 + M^2} - 1\right)^{-1/2}, \tag{34}$$

$$\lambda(\omega) = L\left(\sqrt{1 + M^2} - 1\right)^{1/2}, \tag{35}$$

where

$$L = \omega\sqrt{\frac{1 + \delta\omega^2}{2(1 + \omega^2)}}, \quad M = \frac{(1 - \delta)\omega}{1 + \delta\omega^2}. \tag{36}$$

The frequency dependencies $k(\omega) = \mathrm{Re}(\kappa)$ and $\lambda(\omega) = \mathrm{Im}(\kappa)$ of dispersion relation (24) are displayed in Fig. 2 for the various values of the material parameter δ. Parameter δ can have values on the interval $\delta = [0, 1]$.

If $\delta = 1$, then from (34) and (35) one can find

$$k(\omega) = \omega, \quad \lambda(\omega) = 0. \tag{37}$$

This real valued nondispersive case is evident from the study of expression (10). Because $\gamma = 1 - \delta = 0$, it follows that $\mathcal{R}(t) = 0$, and instead of Eq. (10), we are left with the constitutive equation in the form (11). This form is not dependent on the rate of the felt loading. In fact, Eq. (11) describes a usual elastic material, in which the wave propagates without attenuation.

In case of $\omega \to \infty$, it is easy to see that $k(\omega) \to \omega\sqrt{\delta}$ and that

$$\lim_{\omega\to\infty} \lambda(\omega) = \frac{1 - \delta}{2\sqrt{\delta}}. \tag{38}$$

For large frequencies, the exponential decay constant λ depends only on the parameter δ.

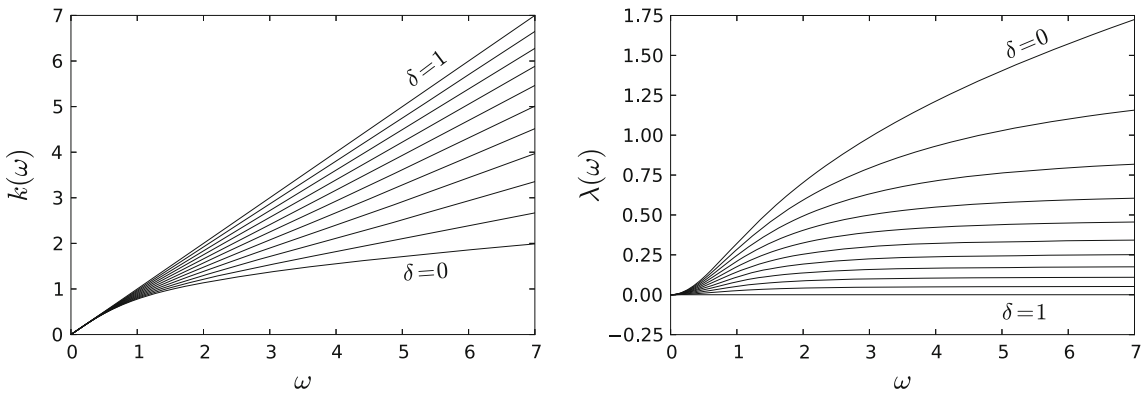

Fig. 2 Dispersion relations $k(\omega)$ and $\lambda(\omega)$ for various values of parameter δ in range [0.0, 1.0] with step 0.1

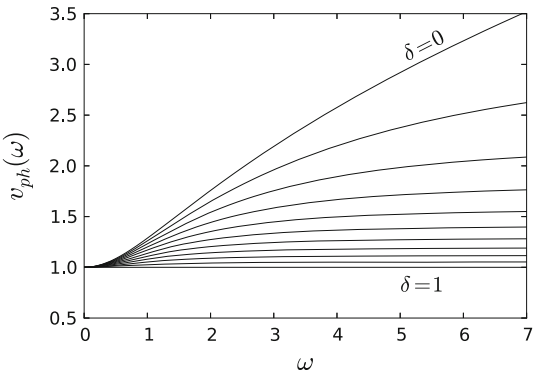

Fig. 3 Phase velocity as a function of frequency for various values of the parameter δ in range [0.0, 1.0] with step 0.1

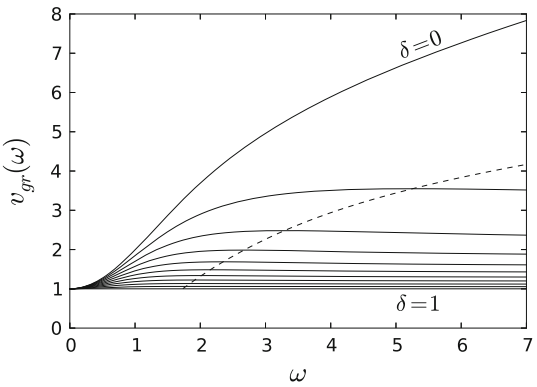

Fig. 4 Group velocity as a function of frequency for various values of the parameter δ in range [0.0, 1.0] with step 0.1. The maximum of v_{gr} for $\delta < 1$ is shown by a *dashed line*

The phase velocity is defined as $v_{ph}(\omega) = \omega/k$, and it takes the following general form:

$$v_{ph} = \frac{\sqrt{2(1+\omega^2)(N-\delta\omega^2-1)}}{(1-\delta)\omega}, \tag{39}$$

where

$$N = \sqrt{(1+\omega^2)(1+\delta^2\omega^2)}. \tag{40}$$

The frequency dependence $v_{ph}(\omega)$ for various values of parameter δ is shown in Fig. 3. In case of $\delta = 1$, the phase velocity becomes $v_{ph}(\omega) = 1$ [cf. relationship (37)]. For large frequencies, the phase velocity has a limit

$$\lim_{\omega\to\infty} v_{ph}(\omega) = \frac{1}{\sqrt{\delta}}. \tag{41}$$

Taking into account (16) and (17), the range of dimensional values of the phase velocity is $c_s \leqslant v_{ph} < c_d$.

The group velocity, which is defined as $v_{\mathrm{gr}}(\omega) = \mathrm{d}\omega/\mathrm{d}k = (\mathrm{d}k/\mathrm{d}\omega)^{-1}$, takes in this case the following general form:

$$v_{\mathrm{gr}} = \frac{2(1+\omega^2)^2\sqrt{2(1+\delta^2\omega^2)}\left(N-\delta\omega^2-1\right)^{3/2}}{\omega(1-\delta)[(1+3\delta^2)\omega^4-(2N+2\delta N-3\delta^2-5)\omega^2-4(N-1)]}, \tag{42}$$

where N is defined by relation (40). The frequency dependence $v_{\mathrm{gr}}(\omega)$ for various values of the parameter δ is presented in Fig. 4. In case of $\delta = 1$, the group velocity $v_{\mathrm{gr}}(\omega) = 1$ [cf. relationship (37)]. For large frequencies, the group velocity has the same limit as the phase velocity has,

$$\lim_{\omega\to\infty} v_{\mathrm{gr}}(\omega) = \frac{1}{\sqrt{\delta}}. \tag{43}$$

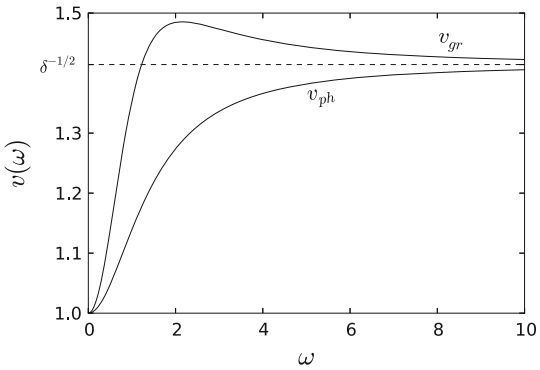

Fig. 5 Comparison of group and phase velocities for a single value of the parameter $\delta = 0.5$. The *dashed line* shows the limit for the large frequencies

The essential difference between the behavior of phase and group velocities is that the phase velocity is a monotonic function of frequency, while the group velocity has a maximum. The maximum of different values of δ is located on the dashed line shown in Fig. 4. A comparison of the two velocities for a single value of δ is presented in Fig. 5. In the wool felt, the group velocity is larger than the phase velocity for any positive frequency. This means that the felt is a material with anomalous dispersion. This fact is true for $\delta < 1$ because as mentioned above, if $\delta = 1$, then $v_{\mathrm{gr}} = v_{ph} = 1$, and we have nondispersive case.

6 Numerical solution of the boundary value problem

The aim of this study was to analyze the one-dimensional deformation (strain) wave propagation inside the felt material along the x axis. This calls for the solution of the boundary value problem of Eq. (19). A boundary value of the strain prescribed at $x = 0$ is selected in the following form:

$$\epsilon(0,t) = A\left(\frac{t}{t_0}\right)^3 \mathrm{e}^{3(1-t/t_0)}, \tag{44}$$

where t_0 defines the time coordinate corresponding to the maximum of a pulse amplitude. This form of a pulse is continuous and smooth. The front of a pulse satisfies the necessary conditions $\epsilon(0,0) = \epsilon_t(0,0) = \epsilon_{tt}(0,0) = 0$.

The solution to this problem is obtained numerically by applying the finite difference method. A more suitable form of Eq. (19) for the finite difference approximation can be obtained by integrating Eq. (19) over time. This yields

$$\epsilon_{tt} = (\epsilon^p)_{xx} - \gamma \int_0^t (\epsilon^p)_{xx}\, \mathrm{e}^{\xi - t}\mathrm{d}\xi, \tag{45}$$

where $\gamma = 1 - \delta$. Initially ($t \leqslant 0$), the felt material is assumed to be at rest, thus $\epsilon(x,0) = \epsilon_t(x,0) = 0$.

Further, the solution of the boundary value problem (45), (44) is presented and analyzed.

6.1 Linear case

Figure 6 shows the numerical solution of the boundary value problem (45) and (44), with the nonlinearity parameter $p = 1$. A pulse propagates through the felt material in the direction of the x-axis. The form of a pulse determined by the boundary value (44) is presented for three sequential time moments, and for three different values of parameter δ. The dashed lines show corresponding decays of pulse amplitudes. These curves are plotted through the pulses' maxima.

The numerical results presented in Fig. 6 are calculated for a pulse with boundary value where the parameter $t_0 = 1/2$. The additional calculations were also repeated for the boundary values where $t_0 = 1$ and $t_0 = 1/3$.

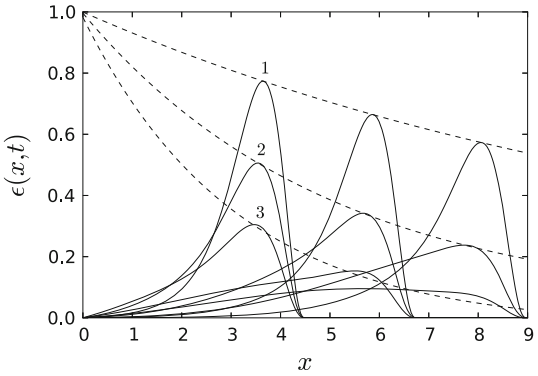

Fig. 6 Snapshots of the pulses' profiles shown for time moments $t = 4.5$, $t = 6.75$, and $t = 9.0$, varying the parameter δ. The boundary value parameter $t_0 = 1/2$. The *dashed lines* show the amplitude decay. For a pulse 1 ($\delta = 0.8$), the corresponding amplitude decay function is $\mathrm{e}^{-0.08x}$; for a pulse 2 ($\delta = 0.5$), the amplitude decay function is $\mathrm{e}^{-0.20x}$; for a pulse 3 ($\delta = 0.2$), the amplitude decay function is $\mathrm{e}^{-0.32x}$

Table 1 Comparison of exponential decay constants λ for different values of parameter δ and frequency ω

δ	t_0	ω	$\lambda(\omega)$	λ_{num}	$\lvert\lambda(\omega) - \lambda_{\mathrm{num}}\rvert$
0.2	1	1	0.246	0.304	0.058
	1/2	2	0.493	0.321	0.172
	1/3	3	0.632	0.361	0.271
0.5	1	1	0.142	0.184	0.042
	1/2	2	0.254	0.201	0.053
	1/3	3	0.300	0.214	0.086
0.8	1	1	0.053	0.068	0.015
	1/2	2	0.087	0.077	0.010
	1/3	3	0.099	0.082	0.017

Here, we suppose that the *fundamental* spectral component ω of a pulse (44) is estimated from relationship $\omega t_0 \simeq 1$. This is a rough approximation, but below, it is shown that the resulting numerical calculations are in agreement with the dispersion analysis.

Table 1 displays the parameter δ, the boundary value parameter t_0, the corresponding value of frequency ω, the value of $\lambda(\omega)$, the value of exponential decay constant λ_{num}, and the absolute value of the difference between λ and λ_{num}. We conclude that the results presented in Table 1 for all values of δ are sufficient enough to confirm that the values of numerically calculated decay constants λ_{num} and the exponential decay constant λ defined by relation (35) are approximately the same. This means that in principle this approach can be used to verify the decay constants for any specific value of t_0 rather accurately.

6.2 Nonlinear case

In this section, the effects of the nonlinearity of the wool felt model on the wave propagation are considered. We examine the influence of the nonlinearity parameter p, and the effect of an initial pulse amplitude A on the evolution of the wave form during its propagation through the felt material.

Figure 7 shows the numerical solution of the boundary value problem (45) and (44). The solution of the problem is presented for three sequential time moments, and for three different values of the nonlinearity parameter p. In this example, the amplitude $A = 0.1$ of the boundary value is a constant for all cases presented.

In Fig. 7, it is possible to see that the front of a pulse becomes steeper as it propagates through the felt material. This pulse steepening increases with the growth of the value of the parameter p. It means that the group velocity is larger than the phase velocity. This phenomenon confirms our conclusion that the felt is a material with anomalous dispersion (*vide* Fig. 5).

The effect of an initial pulse amplitude A on a pulse evolution is presented in Fig. 8. The numerical solution is presented for three sequential time moments, and for three different values of the initial amplitude A of the boundary value (44). It is possible to see that a forward-facing slope of a pulse is strongly dependent on the pulse amplitude A. For larger amplitudes, the maximum point or the crest of a pulse (shown by bullets)

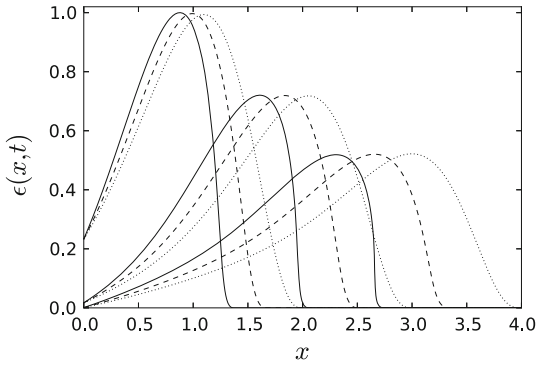

Fig. 7 Evolution of a nonlinear pulse ($t_0 = 1/2$, $A = 0.1$) for three sequential time moments $t = 2$, $t = 3$, and $t = 4$. Material parameters selected $\delta = 0.2$, $p = 1.5$ shown by *solid line*, $p = 1.25$ shown by *dashed line*, $p = 1.0$ (linear case) shown by *dotted line*. Results are normalized

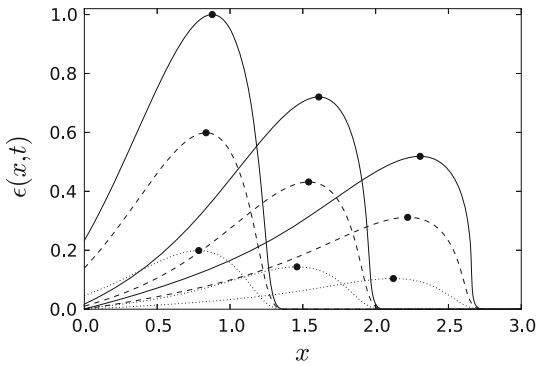

Fig. 8 Evolution of a nonlinear pulse ($t_0 = 1/2$) for three sequential time moments $t = 2$, $t = 3$, and $t = 4$. Material parameters selected $\delta = 0.2$, $p = 1.5$, initial amplitude $A = 0.1$ shown by *solid line*, $A = 0.06$ shown by *dashed line*, $A = 0.02$ shown by *dotted line*. *Bullet* show the position of maximum. Results are normalized

propagates faster than the front of a pulse. Accumulation of this effect results in the eventual pulse breaking. This means that eventually the shock wave will be formed. To simulate this phenomenon, our numerical scheme must be adjusted to the purpose of description of the propagation of discontinuities on the wave front. A detailed analysis of this problem is in progress.

The progressive forward leaning of a propagating pulse can be explained by the fact that the group velocity is larger than the phase velocity. Also, this phenomenon is related to nonlinear features of the felt material and increases with the increase of the amplitude of the initial boundary disturbance.

The animations of the simulated wave pulses propagation through the felt discussed in Sect. 6 are available for viewing at the supplementary Web page of this article.[1]

7 Conclusions

We have derived a nonlinear constitutive equation of microstuctured wool felt based on the experimental results of piano hammers testing. Using this model, the boundary value problem that describes the propagation of deformation waves in the felt material is considered in the current study. In case of the linear felt-type material, the dispersion analysis of the model is carried out, and the dependencies of the phase and group velocities on the felt parameters are obtained. It is shown that the group velocity is always larger than the phase velocity, and therefore, the wool felt is a medium with anomalous dispersion.

The numerical solution of the linear boundary value problem is used to estimate a strain pulse amplitude decay during its propagation through the felt. It is shown that in the linear case the decay constants may be obtained rather accurately by using dispersion analysis.

[1] Supplementary web page of the article: http://www.cs.ioc.ee/~dima/feltdeform.html.

A strain pulse propagation in nonlinear felt is also considered. The general influence of the nonlinear parameter p on a pulse evolution is investigated. It is concluded that the front of a pulse becomes steeper as it propagates through the felt material and that this pulse steepening increases with the growth of the value of the parameter p.

The effect of an initial pulse amplitude A on the nonlinear wave propagation is simulated. It is shown that for larger amplitudes the maximum point or the crest of a pulse propagates faster than the front of a pulse. This is related to the fact that the group velocity is larger than the phase velocity and confirms our assumptions about the felt as a medium with anomalous dispersion.

It is revealed that the front slope of a pulse is strongly determined by a pulse amplitude A. Such a process results in the formation of the shock wave, which is directly caused by the nonlinear features of the microstructured felt material. The originality of the presented model is expressed in the fact that the parameter p that describes the felt nonlinearity may be any real number >1, including the noninteger values. The solution of the novel wave Eqs. (18) and (19) reflects many physical effects as demonstrated in this paper. In conclusion, we may state that the wool felt is a strongly dissipative and dispersive nonlinear medium, with a strong damping effect.

Acknowledgments This research was supported by the EU through the European Regional Development Fund, and by the Estonian Ministry of Education and Research (SF 0140077s08). The authors would like to thank Prof. Aleksander Klauson from Tallinn University of Technology for his assistance in the stress–strain testing of the felt pads.

References

1. Ghosh, M.: An experimental study of the duration of contact of an elastic hammer striking a damped pianoforte string. Indian J. Phys. **7**, 365–382 (1932)
2. Hall, D.E., Askenfelt, A.: Piano string excitation. V. Spectra for real hammers and strings. J. Acoust. Soc. Am. **83**, 1627–1638 (1988)
3. Yanagisawa, T., Nakamura, K., Aiko, H.: Experimental study on force–time curve during the contact between hammer and piano string. J. Acoust. Soc. Jpn. **37**, 627–633 (1981)
4. Yanagisawa, T., Nakamura, K.: Dynamic compression characteristics of piano hammer. Trans. Music. Acoust. Tech. Group Meet. Acoust. Soc. Jpn. **1**, 14–18 (1982)
5. Yanagisawa, T., Nakamura, K.: Dynamic compression characteristics of piano hammer felt. J. Acoust. Soc. Jpn. **40**, 725–729 (1984)
6. Stulov, A.: Hysteretic model of the grand piano hammer felt. J. Acoust. Soc. Am. **97**, 2577–2585 (1995)
7. Rabotnov, Yu.N.: Elements of Hereditary Solid Mechanics, Chap. 17. MIR Publishers, Moscow (1980)
8. Stulov, A., Magi, A.: Piano hammer testing device. Proc. Estonian Acad. Sci. Eng. **6**, 259–267 (2000)
9. Stulov, A.: Experimental and computational studies of piano hammers. Acta Acoust. United Acoust. **91**, 1086–1097 (2005)
10. Stulov, A.: Dynamic behavior and mechanical features of wool felt. Acta Mech. **169**, 13–21 (2004)